Identification of residue inversions in large phylogenies of duplicated proteins

Stefano Pascarelli[1], Paola Laurino[1*]

[1] Protein Engineering and Evolution Unit, Okinawa Institute of Science and Technology Graduate University, Onna, Okinawa 904-0495 Japan.

* Corresponding author

E-mail: paola.laurino@oist.jp

Abstract

Connecting protein sequence to function is becoming increasingly relevant since high-throughput sequencing studies accumulate large amounts of genomic data. In order to go beyond the existing database annotation, it is fundamental to understand the mechanisms underlying functional inheritance and divergence. If the homology relationship between proteins is known, can we determine whether the function diverged?

In this work, we analyze different possibilities of protein sequence evolution after gene duplication and identify "residue inversions", i.e., sites where the relationship between the ancestry and the functional signal is decoupled. Residues in these sites are masked from being recognized by other prediction tools. Still, they play a role in functional divergence and could indicate a shift in protein function. We develop a method to specifically recognize residue inversions in a phylogeny and test it on real and simulated datasets. In a dataset built from the Epidermal Growth Factor Receptor (EGFR) sequences found in 88 fish species, we identify 19 positions that went through inversion after gene duplication, mostly located at the ligand-binding extracellular domain.

Our work uncovers a rare event of protein divergence that has direct implications in protein functional annotation and sequence evolution as a whole. The developed method is optimized to work with large protein datasets and can be readily included in a targeted protein analysis pipeline.

Background

Proteins perform their function either through protein-protein interactions, protein-ligand interactions, or catalyzing chemical reactions. At the molecular level, residues of a protein interact with a counterpart, namely a ligand (small molecule, protein, DNA/RNA, etc.). Herein

51 we define such interacting residues as functional residues. The importance of predicting
52 functional residues in a protein is evident as these residues can contribute to designing new
53 functions, switching specificities, defining protein families and subfamilies, or identifying the
54 occurrence of a functional innovation (e.g., a change of ligand specificity). Crystal structures
55 in which the protein of interest was co-crystallized with its ligand, can readily identify
56 functional residues. However, when the structure is not available, the identification of
57 functional residues is not trivial. Previous attempts used the evolutionary information found in
58 protein sequences and their homologs (1-3), approaches now facilitated by the global-scale
59 genome sequencing effort driven by the development of high-throughput sequencing
60 technologies. The prediction of functional residues by such methods is hampered by the
61 presence of neutral mutations, namely amino acid substitutions that are neither beneficial nor
62 disadvantageous (4). Non-synonymous neutral mutations are on average 10 times more
63 abundant than advantageous mutations (5). While neutral mutations help to determine the
64 phylogenetic position of a protein, mutations of functional residues are a signal of functional
65 shifts that might occur independently of the phylogeny. When the relationship between
66 phylogeny and function is decoupled, neutral mutations may mislead homology-based
67 prediction methods, which are the most common way of functional prediction (6).
68 An event that often decouples the phylogenetic and functional signal is gene duplication. After
69 gene duplication, two proteins follow a semi-independent evolution. For example, before
70 diverging, the two duplicates may influence each other by gene conversion (7) or homomeric-
71 heteromeric interactions (8), and they tend to diversify in the expression profile (9, 10). Gene
72 duplication is prevalent in all domains of life (11), and often the duplicated proteins are
73 reported to go through functional diversification (12). For example, in an event termed "sub-
74 functionalization", a protein with multiple functions (e.g., cellular receptors binding multiple
75 ligands) might split its functions between the two gene copies after duplication. Previously,

76 McClintock *et al.* showed that, in zebrafish HOX genes, the subset of functions inherited by
77 the duplicated copies is different between fish and mouse – a phenomenon named "function
78 shuffling" (13). In cases alike, the phylogenetic signal is misleading when used to predict the
79 function of a "shuffled" orthologous protein. However, if the functional divergence is correctly
80 identified, it allows to highlight the functional residues responsible for this transition, with
81 reduced noise from the neutral variants. In this work, we address the identification of protein
82 functional residues that are mutated during this type of functional rearrangement.
83
84 Residues responsible for a change of function within a protein family are usually called
85 Specificity Determining Sites (SDS). SDS can be predicted by multiple methods (14). SDS
86 prediction methods use the Multiple Sequence Alignment (MSA) or the 3D structure of the
87 protein of interest to calculate a score based on conservation (15-23), evolutionary rate (24-
88 26), or 3D structure properties (27). Most of these approaches require the user to provide the
89 correct groupings of the homologous proteins. When this information is missing, the groupings
90 are made according to the ortholog classification obtained by manual or automatic partitioning
91 methods (28-31). However, the SDS predictions in automatically partitioned orthologs showed
92 a lower sensitivity (32), demonstrating that an incorrect grouping negatively influences the
93 prediction. The grouping usually follows the ortholog conjecture, namely that orthologs are
94 more conserved than paralogs (33, 34). When this is not true, the SDS prediction is hampered.
95 Therefore, the power to predict functional residues is limited by our ability to track protein
96 function on the phylogenetic tree when it is not linearly inherited by orthologs. In our work we
97 address this problem by identifying a signal of functional transition that might prove to be
98 useful when annotating orthologs.
99

EGFR (Epidermal Growth Factor Receptor) is a tyrosine-kinase receptor that activates multiple signaling pathways after binding one of the seven EGFR ligands (35). EGFR is broadly expressed (36) and plays a crucial role in several aspects of organismal development and homeostasis like cellular growth, differentiation, metabolism, and motility (37). In fish, two copies of EGFR were kept after the Teleost-Specific Genome Duplication (TSGD) event that occurred about 350 mya in the actinopterygian lineage (38, 39). Lorin *et al.* showed that both copies of EGFR might have been retained because they are involved in the complex process of skin pigmentation (40), which is under high evolutionary pressure in most fish. Furthermore, the extracellular domain of fish EGFR, responsible for binding multiple ligands, likely went through sub-functionalization (41). For these reasons, EGFR constitutes a perfect model to study uneven functional inheritance events.

In this work, we observe a scenario where the function of a protein is not linearly inherited across orthologs, and we identify the functional residues responsible for the shift of functions. Our goal is to develop an algorithm that highlights the signature of a putative inversion of function, as could be an inversion of residues between the paralogs within the same species. First, we obtain a simple theoretical model that describes the likelihood of a residue inversion in comparison to other outcomes. Then, based on the model, we develop an algorithm that identifies residue inversions in a phylogeny, and we apply it in the context of fish EGFR duplication. Finally, we validate the results using statistical scores and simulated evolution. Our analysis shows a new way to investigate an important and understudied outcome of gene duplication.

Results and Discussions

Theoretical model for residue inversion identification

First, we constructed a simplified model to describe the evolution of a residue through a protein phylogeny after gene duplication and speciation. In the model, a tree branch (b1–b6) could be either mutation (1) or no-mutation (0) state, while a leaf node (Xa, Ya, Xb, Yb) has the possible states 0, 1, or 2 depending on the number of mutations in the preceding branches (Figure 1A). A configuration of six branch states univocally leads to a configuration of four leaf nodes. The model uses two branch length parameters, pre-speciation (t1) and post-speciation (t2), to calculate the probability of each of the 64 branch configurations. Using the model and a set of matching rules between the leaves (Figure 1B), we assessed the probability of seven categories/scenarios of configurations (Figure 1C): *Conserved*, all four residues match; *Type 1* divergence, residues match in only one paralog group; *Type 2* divergence, residues match per paralog group but not per species; *Recent divergence*, all residues match except for one leaf node; *Inversion*, residues of opposite paralog group match but not per species; *Species-specific adaptation*, residues match per species, but not per paralog group; and *Non-conserved*, collecting all events that do not fall in any of the other categories. We used the following formula to calculate the probability of each category:

$$P_{cat} = \sum_{s}^{N} P_{conf} * P_{(cat|conf)}$$

Where N are the 64 configurations of branch states, the probability P_{conf} of the branch configuration is given by the model (Figure S4), and the conditional probability for the category $P_{(cat|conf)}$ is determined by the category's matching rules.

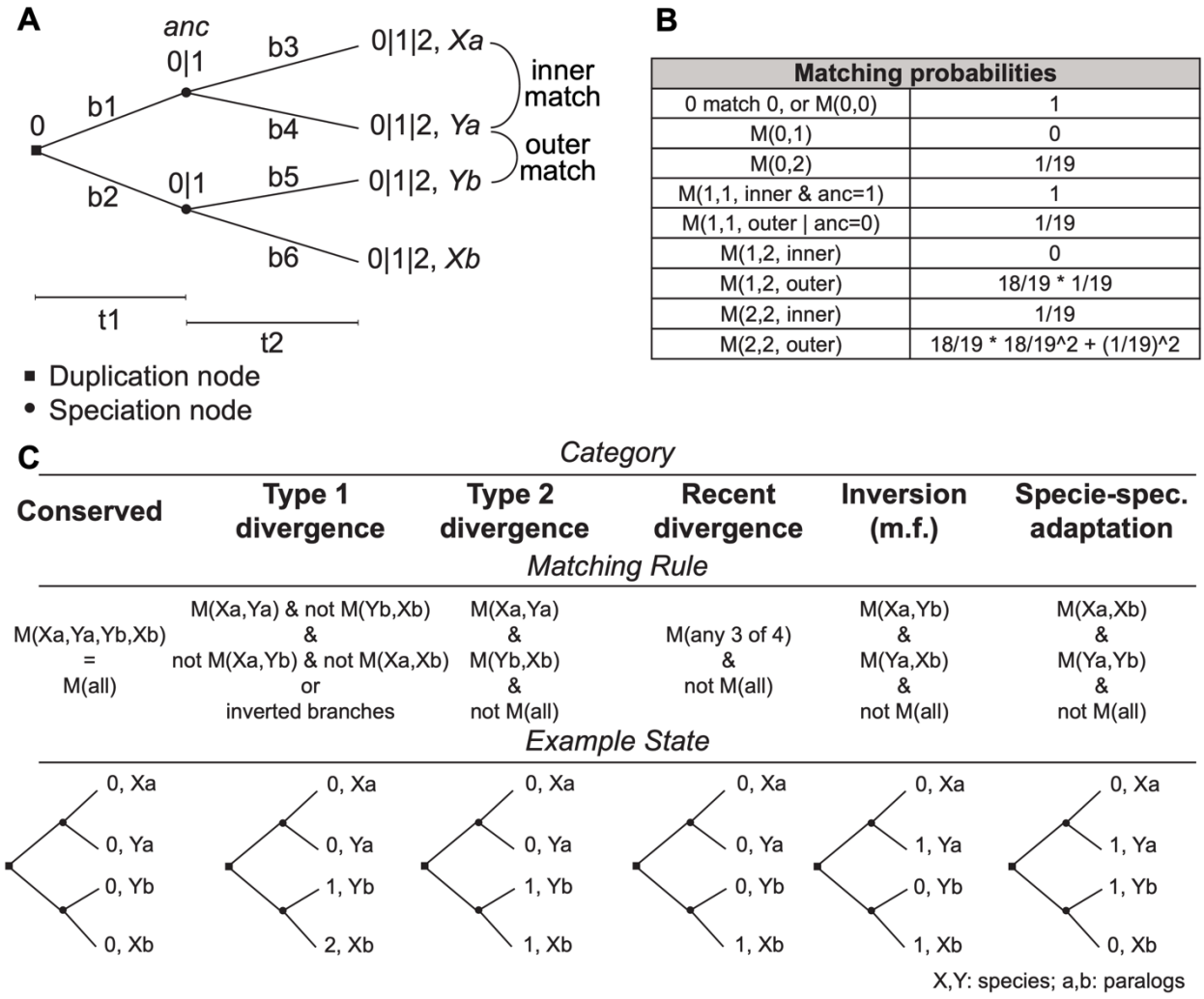

Matching probabilities	
0 match 0, or M(0,0)	1
M(0,1)	0
M(0,2)	1/19
M(1,1, inner & anc=1)	1
M(1,1, outer | anc=0)	1/19
M(1,2, inner)	0
M(1,2, outer)	18/19 * 1/19
M(2,2, inner)	1/19
M(2,2, outer)	18/19 * 18/19^2 + (1/19)^2

Figure 1. Theoretical model of the evolution of protein residue after gene duplication. (A) The structure of the phylogenetic tree that the model is based on. The branch lengths t1 and t2 are used to determine the probability of a mutation on each branch b1 to b6. A leaf node can be found in states 0, 1, or 2 depending on the number of mutations in the preceding branches. An inner match is defined to be a match between orthologs (Xa to Ya, or Xb to Yb), while an outer match is any other match. The probability for a match between two states is given by the table in **(B)** and represents the underlying transition to any of the 20 amino acids. **(C)** Description of the categories. The categories represent a biologically interpretable situation, suggested by their name. Given a certain outcome configuration of states, it is possible to calculate the probability of observing a certain category by using the matching rule. The

157 “Example State” section shows the leaf configuration that gives the highest probability of
158 observing the category described.
159
160 Next, we tested the probability of each category at varying branch lengths (Figure 2A). As
161 expected, short branch lengths lead to a high probability of conserved residues, and long branch
162 lengths lead to non-conserved residues. When the pre-speciation branch length is the longest
163 of the two, we observe a high probability of Type 1 and Type 2 divergence. Whereas, when
164 the post-speciation branch length is the longest, we observe a high probability of recent
165 divergence. Interestingly, for any branch length combination, the two categories of inversion
166 and species-specific adaptation have less than a 1% chance of appearing. From this analysis,
167 we expect to rarely find these two events in real data.

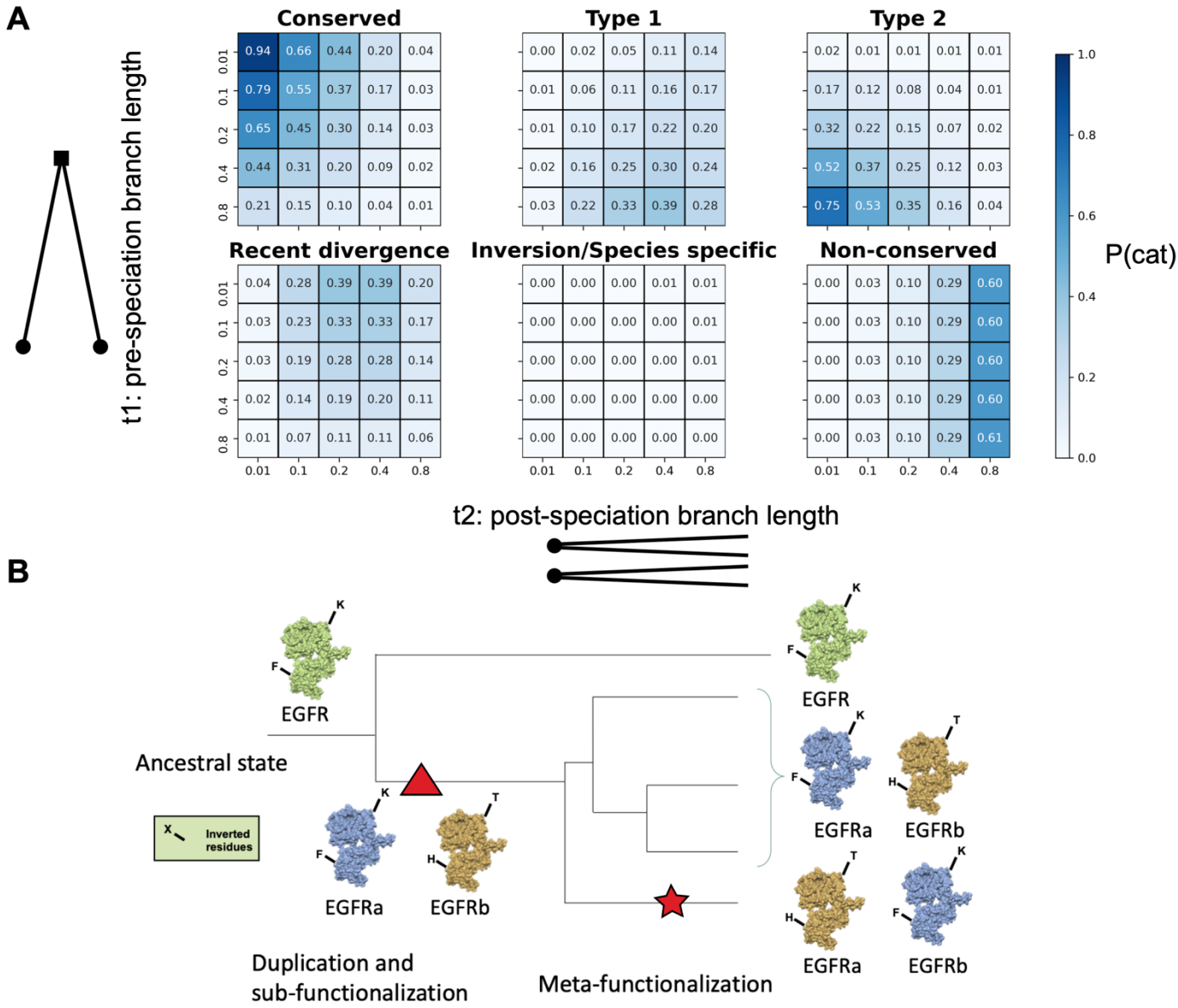

Figure 2. Theoretical model results. (A) The heatmaps show the category probabilities at different tree branch lengths as calculated using the theoretical model definitions. **(B)** Exemplification of "Meta-functionalization" (star), the putative driver of residue inversions in the phylogeny. A multifunctional protein (green) subdivides its functions (blue and yellow) between the two copies obtained after gene duplication (triangle). In a sub-group of species, the functional inheritance of the two copies is inverted. This event is revealed by the pattern of inverted residues compared to the majority of the other species.

177 From the previous results, residues inversions should not be recurrent in a phylogeny. Thus, an
178 unlikely high presence of inverted residues may show that: 1) these residues are following a
179 selective pressure directly related to the paralog function that, for a particular subgroup of
180 species, is opposite and complementary to the other species; or 2) these residues act as
181 compensatory mutations. A recurrent residue inversion could be the proxy of a functional
182 rearrangement between the paralogs within a clade. A rearrangement of functions is facilitated
183 in, but not limited to the Innovation Amplification Divergence (IAD) model of duplicates
184 divergence (42), where paralogs partially retain their secondary functions. We describe this
185 subgroup-specific functional inversion event as a possible outcome after the sub-
186 functionalization of a duplicated gene and we suggest the name "meta-functionalization" from
187 the Greek word "metathesis", namely "put in a different order" (Figure 2B).
188

189 **Algorithm for the identification of residue inversions**

190 We developed an algorithm to identify the events of inversion in a protein phylogeny using a
191 multiple sequence alignment (MSA) and a phylogenetic tree. The algorithm was implemented
192 as a python package named DIRphy, for the Detection of Inverted Residues in a phylogeny.
193 DIRphy splits the protein sequences of the MSA into four groups according to the organism
194 and orthology annotations, which can be either provided by the user or automatically done
195 using a tree distance parameter. Based on the matching probabilities of the previous theoretical
196 model, DIRphy calculates a score for each event of "Inversion" and "Species-specific
197 adaptation", representing its probability to occur (see methods for details). However, for this
198 paper, we will focus only on the inversion events. The output of DIRphy is a list of positions
199 above a defined threshold. When the organism grouping is manually selected, the script
200 calculates both the observed and the expected probability of inversion between the specified
201 groups in the given tree. Otherwise, when the organism grouping is not specified, the output

202 table shows the observed probability of residue inversion given by the grouping that has the
203 highest probability in that position. In the current version of DIRphy, only a binary paralog
204 classification is allowed. DIRphy is released as an open-source project in Github:
205 https://github.com/OISTpasca/protein-inversions
206
207 **Construction of a fish EGFR dataset and identification of residue inversions**
208 We tested DIRphy in the phylogenetic tree of the Epidermal Growth Factor Receptor (EGFR)
209 in the fish lineage. First, we filtered 88 fish genomes (taxon 41665) from the European
210 Nucleotide Archive (ENA) (43) to obtain a dataset of 167 fish EGFR protein sequences. The
211 dataset included all high-quality (N50 > 1Mb) teleost genomes plus one outgroup before the
212 TSGD (spotted gar). From the phylogenetic analysis of this dataset (Supplementary figure 1),
213 three clear duplication events can be observed. The first, most ancient duplication coincided
214 with the TSGD, around the time of the split with gars (~350 mya), and resulted in the separation
215 of the two copies: EGFRa and EGFRb. Two more copies were found in most salmonids,
216 corresponding to the salmon-specific whole-genome duplication around ~80 mya (44), and one
217 more copy in goldfish, possibly due to the carp-specific whole genome duplication about ~10
218 mya (45). The longer branch lengths of EGFRb (Mann-Whitney test, p-val: 2.305e-11) indicate
219 that EGFRb is evolving more rapidly than its counterpart. Furthermore, the EGFRb gene was
220 more commonly lost. Out of 15 gene loss events, only one species lost EGFRa (*S grahami*),
221 while 14 species lost EGFRb.
222
223 Next, we tested the previously computed phylogeny and MSA of fish EGFR for residue
224 inversions using DIRphy. We decided to compare the Cypriniformes clade with the other
225 teleosts because of the high coverage of genomes in both groups, and a sufficiently long
226 separation between the two groups to allow functional divergence on the protein sequence

227 (Figure 3A). We observed a distribution of the scores that resembles an extreme-value
228 distribution, with most of them below 0.01 (Figure 3B). Using the theoretical model, we
229 calculated that the expected value for the probability of residue inversions in the same tree is
230 0.002, much lower than the score of the 99th percentile of 0.16. This percentile value was used
231 as a threshold to select eight sites, the majority of which (six) were from the EGFR extracellular
232 domain. We highlighted the positions of the six sites on the 3D structure of EGFRa and EGFRb
233 extracellular domain from a representative Cypriniformes (*S. anshuiensis*), modeled using the
234 human structure template (Figure 3C). Of the six selected positions, only one (MSA pos 520)
235 was found at the ligand-binding pocket interface. Pos 520 corresponds to Phe-357 in hEGFR.
236 Previous studies showed that the hydrophobic interaction between Phe-357 and Tyr-13 in the
237 ligand hEGF is determinant for the binding (46). In the fish clade *Xiphophorus*, the observed
238 change between Phe and His at this position is considered to be the determinant cause of the
239 different responses of EGFRa and EGFRb after ligand stimulation (47). Out of the six positions
240 in the extra-cellular domain, two showed a conservative substitution (Figure 3D). MSA
241 position 506 contains hydrophobic and aliphatic amino acids (Ile or Val), while position 491
242 shows a small and uncharged amino acid (Ser or Thr). All other positions exhibited a shift of
243 amino acid physicochemical properties. These results show that DIRphy can identify inverted
244 residues in a protein duplication phylogeny, regardless of the amino acid substitution type.

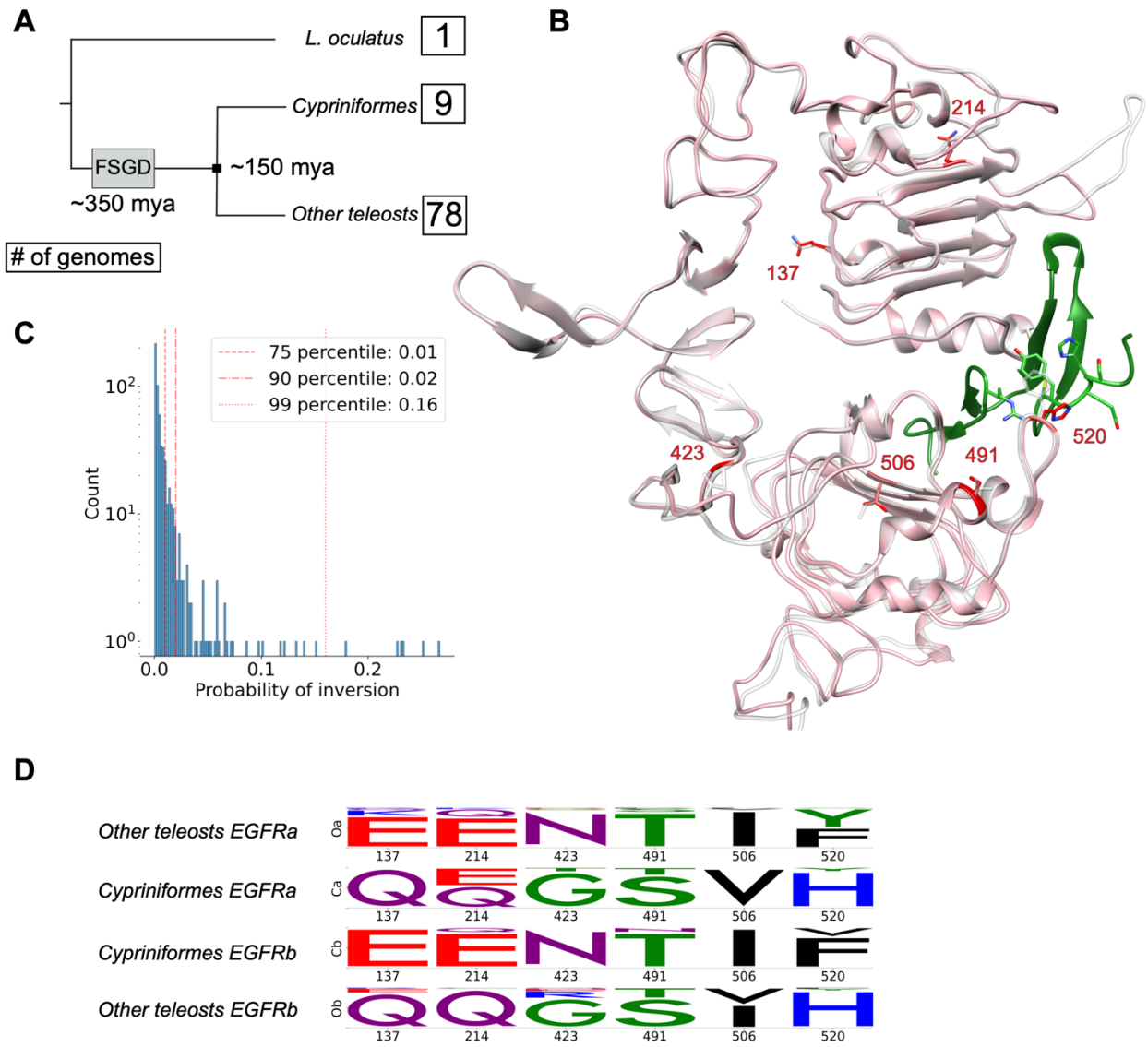

Figure 3. Inverted residues in fish EGFR. (A) Schematic representation of the fish dataset phylogeny. The dates (mya: million years ago) indicate the time of the Fish Specific whole Genome Duplication (FSGD) and the separation of Cypriniformes fish to all other teleost fish. The number in the boxes represents how many genomes are in the dataset for that group. **(B)** 3D model superposition of *S. anshuensis* EGFRa (pink) and EGFRb (white), generated by homology using human EGFR as a template (1IVO) (48). The inverted residues have been highlighted in red. The ligand EGF (green) was taken from the human model after superposing the receptors. **(C)** DIRphy score distribution. The residue inversion probability score was

254 calculated for each site in the MSA that has less than 60% gaps. The top 1% of sites were
255 further characterized. **(D)** Logo representation of the four sub alignments (two species groups,
256 two protein copies) in the inverted residue sites. The logo represents the normalized amino acid
257 count per column and was obtained using the python package Logomaker (49).
258
259 **Score validation by simulated evolution**
260 We statistically validated the score observed in the fish EGFR data using a simulated evolution
261 experiment. In this simulation, random starting amino acids are run through a phylogenetic tree
262 that has the same topology as the previously computed fish EGFR tree. The simulation used
263 the same evolutionary model of the fish EGFR tree to output a MSA as a result. Compared to
264 the fish EGFR MSA, the simulated evolution MSA showed on average lower DIRphy scores
265 while having a similar shape of the score distribution (Figure 4A). No specific amino acid was
266 found to have high scores. Interestingly, the three residues involved in the interaction in
267 position 520 (His, Tyr, and, except for one site, Phe) failed to produce any score higher than
268 0.05 in the simulation (Figure 4B). For further analysis, we used the 99th percentile score of the
269 simulation as a threshold for selecting inverted residues in the real dataset (Supplementary table
270 1, Supplementary figure 2). In summary, the simulated evolution experiment provided a score
271 threshold for detecting residue inversions and confirmed the low chance of this event in the
272 fish EGFR dataset, as observed in the theoretical model.
273
274 **Tree bootstrap**
275 We characterized the phylogenetic information carried by the residue inversions when
276 reconstructing the correct fish EGFR phylogeny tree structure. First, we computed a
277 phylogenetic tree using the sub-alignment of 19 inverted residue sites that score higher than
278 the 99th percentile in the simulated evolution experiment (Supplementary figure 3). In this

279 phylogenetic tree, we can still see two defined groups of sequences corresponding to the two
280 copies of EGFR. Though, as expected, all the sequences from Cypriniformes EGFRa cluster
281 together with the EGFRb group, and vice versa the Cypriniformes EGFRb cluster in the EGFRa
282 group. When we compared this tree to the full-alignment tree, we calculated a similarity value
283 of 74.84 out of 165 using the tree similarity score of Nye *et al.* (50). Next, we generated a pool
284 of bootstrap trees with a reduced alignment length, and we checked their similarity to the full
285 alignment and the inverted residue trees (Figure 4C). We observed a decrease in tree similarity
286 to the full tree proportional to the decrease in alignment length. However, the inverted residue
287 tree distance is statistically less similar to the full alignment tree than the bootstraps, even
288 among the bootstraps with an equivalent length of 20 residues (student t-test p-value: 0.0019).
289 This result suggests that the inverted residues are just a minority of the sites in the alignment
290 and that they disperse the phylogenetic information faster than the average. This view is
291 compatible with the hypothesis that a few functional mutations are hidden behind an
292 overwhelming amount of neutral or nearly-neutral variants, complicating their detection.
293

294 **Comparison of DIRphy inverted residues to Specificity Determining Sites (SDS)**
295 **prediction**

296 We predicted the SDS of fish EGFR using SPEER (32), and observed a marked difference in
297 the type of identified positions compared to DIRphy. To compare the two methods, we defined
298 a "matching probability" as the dot product of the amino acid emission probability vectors of
299 two HMM models. Then, we compared, for each site of the fish EGFR alignment, the mean
300 matching probability between HMM models of the orthologs (cypriniformes EGFRa to other
301 fish EGFRa, and cypriniformes EGFRb to other fish EGFRb) with the mean matching
302 probability between the paralogs (cypriniformes EGFRa to other fish EGFRb, and
303 cypriniformes EGFRb to other fish EGFRa) (Figure 4D). From this analysis, it is evident that

304 SPEER tends to predict sites with a high ortholog-low paralog correlation. These sites are likely
305 to possess a paralog-specific function. On the other hand, DIRphy identifies diametrically
306 opposite sites, with a high paralog-low ortholog correlation. Both types of sites deviates from
307 the diagonal, a pattern that suggests a functional adaptation. However, the sites that show an
308 inversion are more challenging to identify for SDS predictions because, for a subset of species,
309 the conservation pattern is inverted, and the signal is averaged out. In summary, the
310 identification of residue inversion event has the potential to improve functional residue
311 predictions, as DIRphy is able to identify functional sites that are overlooked by SDS prediction
312 methods.

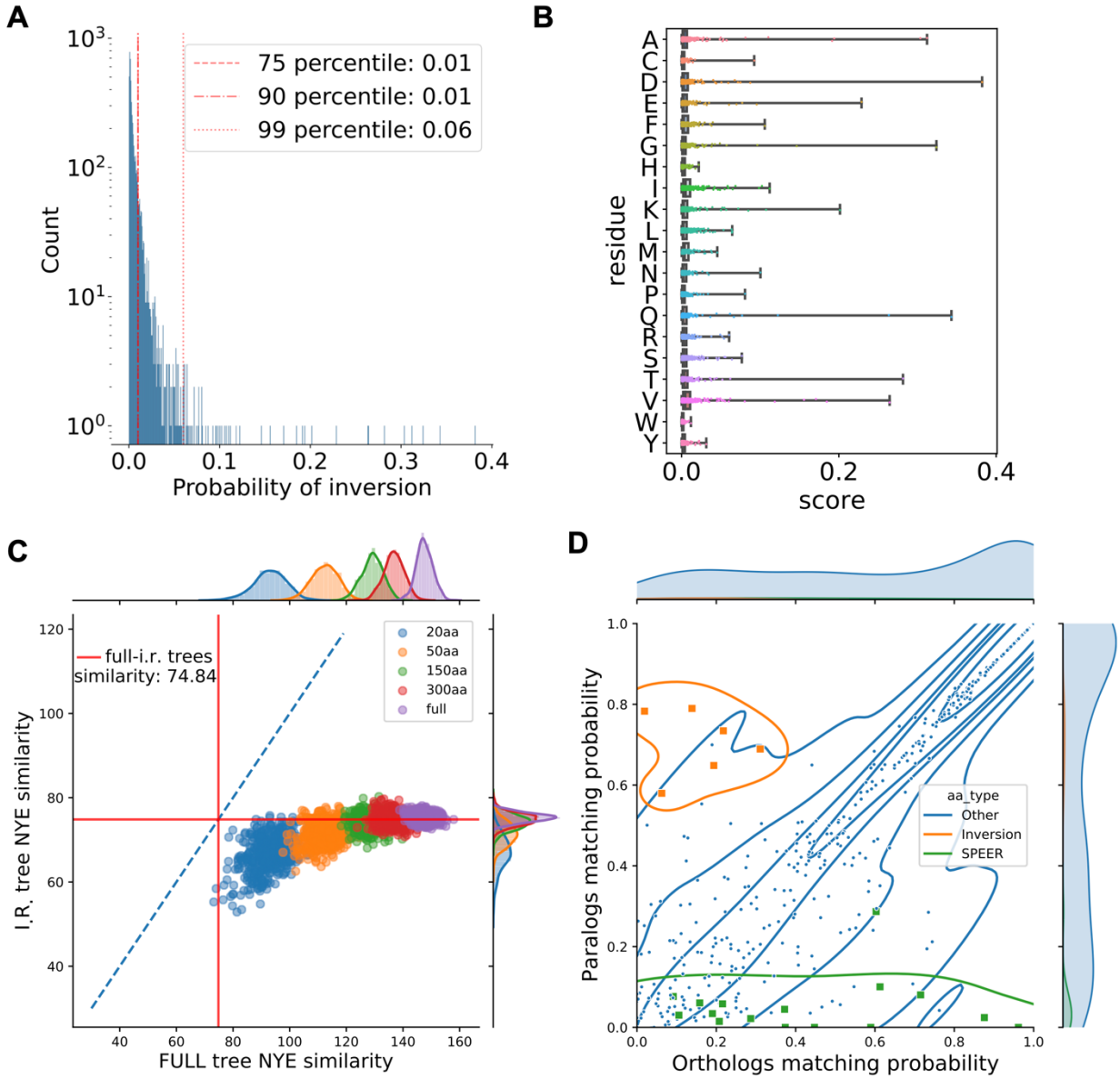

Figure 4. Outcome to the validations. (A) Distribution of the simulated evolution DIRphy scores. A 5000 random amino acid sequence was evolved through the fish EGFR phylogenetic tree using the same evolutionary models used to generate the tree. The resulting MSA was used to compute the DIRphy score. **(B)** Distribution per amino acid of the simulated evolution DIRphy scores as shown by the reference (*S. anshuiensis* EGFRa). **(C)** Bootstrap trees similarity to the full and inverted residue trees. The color represents the length of the sub-alignment used to generate the bootstrap tree. The red line shows the similarity between the full and inverted residue trees. The blue line is the identity line. **(D)**

322 Comparison of the sites identified by DIRphy and SPEER. The matching probability of the
323 HMM of four sub-alignments was used to compare between species the orthologs (EGFRa vs
324 EGFRa, EGFRb vs EGFRb) and paralogs (EGFRa vs EGFRb). The matching probability is
325 calculated as the average of two dot products of the frequency arrays. The orange color
326 shows sites where a residue inversion was identified, while the green color shows sites where
327 the p-value of SPEER score is lower than 0.01.
328
329 **Conclusions**
330 In conclusion, we have detected an event in paralogs that lead to the inversion of functional
331 residues. This new event has been described by a theoretical model and validated by literature
332 and bioinformatics studies. To the best of our knowledge, we are the first to identify and
333 describe the residue inversion event, possibly because this event might be rare. However,
334 residue inversions are potentially exploited for functional divergence and, if missed, might
335 lead to the wrong classification of proteins in the correct functional groups. We provide a
336 general tool, named DIRphy, to identify residue inversions in a large protein dataset. DIRphy
337 can be easily integrated in an existing pipeline of protein annotation to improve functional
338 annotation and provide the positions that might have been overlooked by other functional site
339 prediction methods.
340
341 **Materials and Methods**
342
343 **Theoretical model**
344 The model was built on the following assumptions: 1) equal branch length between the two
345 paralogs: b1 = b2, b3 = b4 = b5 = b6; 2) only zero to one mutation can occur in each of the
346 six branches; 3) after a mutation, each residue is equiprobable; 4) no selective pressure; 5) the

347 probability of a mutation on a branch solely depends on the branch length (mutation rate) and
348 is $P = 1 - e^{-\lambda}$ where P is the probability of a mutation and λ is the mutation rate.
349
350 Given the probability of a mutation in each of the six branches, we can calculate the
351 probability of all the 64 (2^6) configurations of mutations on the tree. A configuration
352 unequivocally leads to a determined leaf node state (Supplementary figure 4). We defined the
353 leaf node states with the allowed values zero, one, or two. The state value represents the
354 number of mutations that happened in the branches connecting to the leaf node (Figure 1A).
355 Then, we defined the probability of a match between leaf nodes based on the state value. The
356 probabilities describe the situation in which a residue can mutate to one of 19 possible other
357 residues. In some cases, the matching probability depends on the state of the ancestral node
358 before speciation, e.g., a single or double mutation in the inner branch leaves. Finally, we
359 defined seven categories based on the type of matching at the leaf nodes, and we defined their
360 probability of occurrence based on the matching probabilities between leaf nodes.
361
362 **Model categories**
363 Here we give a brief description of the model categories and formulas used to calculate their
364 probabilities in the model.
365 <u>*Conserved*</u>
366 $$P_{cons} = mi_{Xa,Ya} * mi_{Xb,Yb} * \max(mo_{Xa,Xb}, mo_{Xa,Yb}, mo_{Ya,Xb}, mo_{Ya,Yb})$$
367 Where *mi* stands for the inner match, *mo* stands for the outer match and corresponds to the
368 probabilities of a match in figure 1B. The conserved category collects the states where a site
369 is invariant in all four leaf nodes. It could arise from no mutations, but also from (two, three,
370 or) four mutations to the same amino acid. In the formula, the maximum value of the outer

matches is used as the best approximation of the conditional probability of matching all leaf nodes given the two inner matches.

Type 1 Divergence

$$P_{type1} =$$

$$= mi_{Xa,Ya} * (1 - mi_{Xb,Yb}) * (1 - \min(mo_{Xa,Xb}, mo_{Ya,Xb})) * (1 - \min(mo_{Xa,Yb}, mo_{Ya,Yb}))$$

$$+(1 - mi_{Xa,Ya}) * mi_{Xb,Yb} * (1 - \min(mo_{Xa,Xb}, mo_{Xa,Yb})) * (1 - \min(mo_{Ya,Xb}, mo_{Ya,Yb}))$$

The type 1 divergence collects the states where the amino acid is matching between species only in one paralog, while there is no match in the other paralog.

Type 2 Divergence

$$P_{type2} = mi_{Xa,Ya} * mi_{Xb,Yb} * (1 - P_{cons})$$

The type 2 divergence collects the states where the two paralogs display a different amino acid but are conserved between species. Type 1 and type 2 classifications are based on (51).

Recent Divergence

$$P_{recent} = sum(mi_{Xa,Ya} * mo_{Xa,Xb} * (1 - mo_{Xb,Yb})$$

$$mi_{Xa,Ya} * mo_{Xa,Yb} * (1 - mo_{Xb,Yb})$$

$$mi_{Xb,Yb} * mo_{Xa,Xb} * (1 - mo_{Xa,Ya})$$

$$mi_{Xb,Yb} * mo_{Ya,Xb} * (1 - mo_{Xa,Ya}))$$

The recent divergence collects the states where only one leaf node is different (diverged) compared to the other three nodes.

Inversion / Specie-Specific Adaptation

$$P_{inv} = mo_{Xa,Yb} * mo_{Xb,Ya} * (1 - \min(mi_{Xa,Ya}, mi_{Xb,Yb}))$$

And similarly,

$$P_{ssa} = mo_{Xa,Xb} * mo_{Ya,Yb} * (1 - \min(mi_{Xa,Ya}, mi_{Xb,Yb}))$$

These two categories represent the states where the amino acid does not match between orthologs but matches between paralogs for the inversion or between species for the species-specific adaptation.

Calculation of inverted residue score

We devised a score to identify inverted residues in a phylogeny. The score was based on the probability of observing an inversion in the previously described model and calculated with the following steps: 1) Divide an MSA into four sub-alignments (two EGFR copies and two species groups). 2) Generate four amino acid frequency arrays, optionally normalized by pseudo-counts*. 3) Calculate the probability of a match between two groups using the dot product of the frequency array. 4) Calculate the joint probability of inversion (or similarly for species-specific adaptation) from the conditional probabilities and the frequency array matching using the following formulas:

$$P_{\overline{(M(Xa,Xb,Ya,Yb)}|M(Xa,Yb),M(Ya,Xb)} = \sum_{i}^{20} \frac{Xa[i] * Yb[i]}{M(Xa,Yb)} * (1 - \frac{Ya[i] * Xb[i]}{M(Ya,Xb)})$$

$$P_{\overline{(M(Xa,Xb,Ya,Yb)},M(Xa,Yb),M(Ya,Xb)} = P_{\overline{(M(Xa,Xb,Ya,Yb)}|M(Xa,Yb),M(Ya,Xb)} * M(Xa,Yb) * M(Ya,Xb)$$

Where *Xa,Xb,Ya,Yb* are the amino acid frequency arrays for the MSA sequence groups with the same names, *i* is the counter spanning each amino acid. The probability of a match (e.g., *M(Xa,Yb)*) is given by the array dot product: $M(Xa,Yb) = \sum_{i}^{20} Xa[i] * Yb[i]$. The latter joined probability represents the inverted residue score.

*** Pseudo-count normalization**

To correct any possible bias given by groups with a small number of species, we implemented a pseudo-count normalization of the amino acid frequency array, as previously

418 done in Tatsuov *et al.* (52). We used the LG protein substitution matrix (53) as background
419 amino acid frequency probability. The value of the beta parameter for the pseudo-counts
420 formula was set by default to five; however, it is possible to modify this parameter before
421 running the pipeline.
422
423 **Fish dataset**
424 To test the inverted residue score, we generated a fish genome dataset. First, we downloaded
425 all genomes from the European Nucleotide Archive (ENA) belonging to taxon 41665
426 (Actinopterygii). Through this method, we obtained 88 fish genomes. Next, we downloaded
427 the pre-annotated fish EGFR protein sequences from the ENSEMBL database (54) and used
428 them to build an HMM profile with the HMMER package (55). The HMM profile was used
429 as a query in Augustus package suite (56) to search for EGFR related genes in the fish
430 genomes. We then filtered out interrupted CDS, sequences clustering with other ErbBs in a
431 phylogenetic tree, and sequences with an aberrant branch length in the non-synonymous
432 codon tree. After this procedure, we obtained 167 fish EGFR protein sequences.
433
434 **Phylogenetic analysis**
435 We performed the phylogenetic analysis of the fish EGFR protein sequences using MAFFT
436 (57) to align the sequences, and IQTREE (58) with ModelFinder (59) to search for the best
437 evolutionary model to generate the phylogenetic tree. To generate the synonymous tree, we
438 used paml CODEML (60).
439
440 **Sequence and structure analysis**

441 The sequences and alignments were handled using Unipro Ugene (61). The protein structure
442 images and analyses were performed with UCSF Chimera (62). The modelling of fish EGFR
443 structures was performed using the SWISS-MODEL web server (63) and AlphaFold 2 (64).
444
445 **Simulated evolution**
446 We ran a simulated evolution experiment using an in-house pipeline based on the Pyvolve
447 python package (65). The pipeline simulated an evolutionary pathway of 5000 random amino
448 acids on the fish EGFR phylogenetic tree, using the same model of evolution and
449 evolutionary rates that were used to construct the tree (JTT with rate heterogeneity) (66-68).
450 The simulation generated an output alignment that was used to run the DIRphy pipeline, to
451 calculate the base probability of an inversion.
452
453 **Bootstrap**
454 To perform the bootstrap, we used an in-house Matlab script. We selected from the fish
455 EGFR DIRphy prediction the 19 sites with a score higher than the 99th percentile of the
456 simulated evolution scores. We calculated a phylogenetic tree for the full alignment and the
457 inverted residues alignment using the neighbor-joining algorithm (69) and the BLOSUM80
458 matrix (70). The similarity distance between trees was calculated using the method described
459 in Nye *et al.* (50). We then performed 500 bootstrap alignments for each set of alignment
460 lengths: full, 250, 100, 20. We excluded columns with 90% or more gaps and repeated the
461 sampling whenever one sequence did not have at least one non-gap position. For each
462 bootstrap alignment, we generated a tree, then calculated the distance to the full tree and
463 inverted residue tree.
464
465

Declarations

Ethics approval and consent to participate

Not applicable

Consent for publication

Not applicable

Availability of data and materials

The data and scripts used to support the conclusions of this article are available in the DIRphy Github python repository: https://zenodo.org/badge/latestdoi/346201641.

Competing interests

The authors declare no competing financial interests.

Funding

Funding support by the Okinawa Institute of Science and Technology to P.L. is gratefully acknowledged.

Author contributions

S.P. and P.L. designed the project. S.P. performed the research. S.P. and P.L. analyzed the data and wrote the manuscript.

Acknowledgments

We thank Federica di Palma, Tarang K. Mehta, and Wilfried Haerty for the thoughtful discussions on fish phylogeny. Stanisław Dunin-Horkawicz and Dan Kozome for critical

reading of the manuscript. We are grateful for the help and support provided by the Scientific Computing and Data Analysis section of Research Support Division at OIST. Financial support by the Okinawa Institute of Science and Technology to P.L. is gratefully acknowledged.

References

1. Ashkenazy H, Abadi S, Martz E, Chay O, Mayrose I, Pupko T, et al. ConSurf 2016: an improved methodology to estimate and visualize evolutionary conservation in macromolecules. Nucleic Acids Res. 2016;44(W1):W344-W50.

2. Sankararaman S, Kolaczkowski B, Sjölander K. INTREPID: a web server for prediction of functionally important residues by evolutionary analysis. Nucleic Acids Res. 2009;37(Web Server issue):W390-5.

3. Wilkins AD, Bachman BJ, Erdin S, Lichtarge O. The use of evolutionary patterns in protein annotation. Curr Opin Struct Biol. 2012;22(3):316-25.

4. Kimura M. The neutral theory of molecular evolution: a review of recent evidence. Jpn J Genet. 1991;66(4):367-86.

5. Rockah-Shmuel L, Tóth-Petróczy Á, Tawfik DS. Systematic Mapping of Protein Mutational Space by Prolonged Drift Reveals the Deleterious Effects of Seemingly Neutral Mutations. PLoS Comput Biol. 2015;11(8):e1004421.

6. Lee D, Redfern O, Orengo C. Predicting protein function from sequence and structure. Nat Rev Mol Cell Biol. 2007;8(12):995-1005.

7. Mitchell MB. ABERRANT RECOMBINATION OF PYRIDOXINE MUTANTS OF Neurospora. Proc Natl Acad Sci U S A. 1955;41(4):215-20.

514 8. Mallik S, Tawfik DS. Determining the interaction status and evolutionary fate of
515 duplicated homomeric proteins. PLoS Comput Biol. 2020;16(8):e1008145.

516 9. Gout JF, Lynch M. Maintenance and Loss of Duplicated Genes by Dosage
517 Subfunctionalization. Mol Biol Evol. 2015;32(8):2141-8.

518 10. Huerta-Cepas J, Dopazo J, Huynen MA, Gabaldón T. Evidence for short-time
519 divergence and long-time conservation of tissue-specific expression after gene duplication.
520 Brief Bioinform. 2011;12(5):442-8.

521 11. Zhang J. Evolution by gene duplication: an update. Trends in Ecology & Evolution.
522 2003;18(6):292-8.

523 12. Innan H, Kondrashov F. The evolution of gene duplications: classifying and
524 distinguishing between models. Nature Reviews Genetics. 2010;11(2):97-108.

525 13. McClintock JM, Kheirbek MA, Prince VE. Knockdown of duplicated zebrafish hoxb1
526 genes reveals distinct roles in hindbrain patterning and a novel mechanism of duplicate gene
527 retention. Development. 2002;129(10):2339-54.

528 14. Chakraborty A, Chakrabarti S. A survey on prediction of specificity-determining sites
529 in proteins. Briefings in Bioinformatics. 2014;16(1):71-88.

530 15. Casari G, Sander C, Valencia A. A method to predict functional residues in proteins.
531 Nat Struct Biol. 1995;2(2):171-8.

532 16. Lichtarge O, Bourne HR, Cohen FE. An evolutionary trace method defines binding
533 surfaces common to protein families. J Mol Biol. 1996;257(2):342-58.

534 17. Panchenko AR, Kondrashov F, Bryant S. Prediction of functional sites by analysis of
535 sequence and structure conservation. Protein Sci. 2004;13(4):884-92.

536 18. Mirny LA, Gelfand MS. Using Orthologous and Paralogous Proteins to Identify
537 Specificity-determining Residues in Bacterial Transcription Factors. J Mol Biol.
538 2002;321(1):7-20.

539 19. Fischer JD, Mayer CE, Söding J. Prediction of protein functional residues from
540 sequence by probability density estimation. Bioinformatics. 2008;24(5):613-20.

541 20. Hannenhalli SS, Russell RB. Analysis and prediction of functional sub-types from
542 protein sequence alignments. J Mol Biol. 2000;303(1):61-76.

543 21. Kalinina OV, Mironov AA, Gelfand MS, Rakhmaninova AB. Automated selection of
544 positions determining functional specificity of proteins by comparative analysis of
545 orthologous groups in protein families. Protein Sci. 2004;13(2):443-56.

546 22. Reva B, Antipin Y, Sander C. Determinants of protein function revealed by
547 combinatorial entropy optimization. Genome Biol. 2007;8(11):R232.

548 23. Wuster A, Venkatakrishnan AJ, Schertler GF, Babu MM. Spial: analysis of subtype-
549 specific features in multiple sequence alignments of proteins. Bioinformatics.
550 2010;26(22):2906-7.

551 24. Abhiman S, Sonnhammer EL. Large-scale prediction of function shift in protein
552 families with a focus on enzymatic function. Proteins. 2005;60(4):758-68.

553 25. Gu X, Zou Y, Su Z, Huang W, Zhou Z, Arendsee Z, et al. An update of DIVERGE
554 software for functional divergence analysis of protein family. Mol Biol Evol.
555 2013;30(7):1713-9.

556 26. Capra JA, Singh M. Characterization and prediction of residues determining protein
557 functional specificity. Bioinformatics. 2008;24(13):1473-80.

558 27. Amitai G, Shemesh A, Sitbon E, Shklar M, Netanely D, Venger I, et al. Network
559 analysis of protein structures identifies functional residues. J Mol Biol. 2004;344(4):1135-46.

560 28. Wicker N, Perrin GR, Thierry JC, Poch O. Secator: a program for inferring protein
561 subfamilies from phylogenetic trees. Mol Biol Evol. 2001;18(8):1435-41.

562 29. Storm CE, Sonnhammer EL. Automated ortholog inference from phylogenetic trees
563 and calculation of orthology reliability. Bioinformatics. 2002;18(1):92-9.

564 30. Zmasek CM, Eddy SR. RIO: analyzing proteomes by automated phylogenomics using
565 resampled inference of orthologs. BMC Bioinformatics. 2002;3:14.

566 31. Li L, Stoeckert CJ, Jr., Roos DS. OrthoMCL: identification of ortholog groups for
567 eukaryotic genomes. Genome Res. 2003;13(9):2178-89.

568 32. Chakraborty A, Mandloi S, Lanczycki CJ, Panchenko AR, Chakrabarti S. SPEER-
569 SERVER: a web server for prediction of protein specificity determining sites. Nucleic Acids
570 Res. 2012;40(Web Server issue):W242-8.

571 33. Tatusov RL, Koonin EV, Lipman DJ. A genomic perspective on protein families.
572 Science. 1997;278(5338):631-7.

573 34. Dolinski K, Botstein D. Orthology and functional conservation in eukaryotes. Annu
574 Rev Genet. 2007;41:465-507.

575 35. Oda K, Matsuoka Y, Funahashi A, Kitano H. A comprehensive pathway map of
576 epidermal growth factor receptor signaling. Mol Syst Biol. 2005;1:2005.0010.

577 36. Yano S, Kondo K, Yamaguchi M, Richmond G, Hutchison M, Wakeling A, et al.
578 Distribution and function of EGFR in human tissue and the effect of EGFR tyrosine kinase
579 inhibition. Anticancer Res. 2003;23(5a):3639-50.

580 37. Hubbard SR, Miller WT. Receptor tyrosine kinases: mechanisms of activation and
581 signaling. Curr Opin Cell Biol. 2007;19(2):117-23.

582 38. Amores A, Suzuki T, Yan YL, Pomeroy J, Singer A, Amemiya C, et al.
583 Developmental roles of pufferfish Hox clusters and genome evolution in ray-fin fish.
584 Genome Res. 2004;14(1):1-10.

585 39. Meyer A, Van de Peer Y. From 2R to 3R: evidence for a fish-specific genome
586 duplication (FSGD). Bioessays. 2005;27(9):937-45.

587 40. Lorin T, Brunet FG, Laudet V, Volff JN. Teleost Fish-Specific Preferential Retention
588 of Pigmentation Gene-Containing Families After Whole Genome Duplications in
589 Vertebrates. G3 (Bethesda). 2018;8(5):1795-806.

590 41. Laisney J, Braasch I, Walter RB, Meierjohann S, Schartl M. Lineage-specific co-
591 evolution of the Egf receptor/ligand signaling system. BMC Evol Biol. 2010;10:16.

592 42. Bergthorsson U, Andersson DI, Roth JR. Ohno's dilemma: evolution of new genes
593 under continuous selection. Proc Natl Acad Sci U S A. 2007;104(43):17004-9.

594 43. Leinonen R, Akhtar R, Birney E, Bower L, Cerdeno-Tárraga A, Cheng Y, et al. The
595 European Nucleotide Archive. Nucleic Acids Res. 2011;39(Database issue):D28-31.

596 44. Macqueen DJ, Johnston IA. A well-constrained estimate for the timing of the
597 salmonid whole genome duplication reveals major decoupling from species diversification.
598 Proc Biol Sci. 2014;281(1778):20132881.

599 45. Wang JT, Li JT, Zhang XF, Sun XW. Transcriptome analysis reveals the time of the
600 fourth round of genome duplication in common carp (Cyprinus carpio). BMC Genomics.
601 2012;13:96.

602 46. Tadaki DK, Niyogi SK. The functional importance of hydrophobicity of the tyrosine
603 at position 13 of human epidermal growth factor in receptor binding. The Journal of
604 biological chemistry. 1993;268(14):10114-9.

605 47. Gomez A, Volff JN, Hornung U, Schartl M, Wellbrock C. Identification of a second
606 egfr gene in Xiphophorus uncovers an expansion of the epidermal growth factor receptor
607 family in fish. Mol Biol Evol. 2004;21(2):266-75.

608 48. Ogiso H, Ishitani R, Nureki O, Fukai S, Yamanaka M, Kim JH, et al. Crystal structure
609 of the complex of human epidermal growth factor and receptor extracellular domains. Cell.
610 2002;110(6):775-87.

611 49. Tareen A, Kinney JB. Logomaker: beautiful sequence logos in Python.
612 Bioinformatics. 2020;36(7):2272-4.

613 50. Nye TM, Liò P, Gilks WR. A novel algorithm and web-based tool for comparing two
614 alternative phylogenetic trees. Bioinformatics. 2006;22(1):117-9.

615 51. Gu X. Maximum-likelihood approach for gene family evolution under functional
616 divergence. Mol Biol Evol. 2001;18(4):453-64.

617 52. Tatusov RL, Altschul SF, Koonin EV. Detection of conserved segments in proteins:
618 iterative scanning of sequence databases with alignment blocks. Proc Natl Acad Sci U S A.
619 1994;91(25):12091-5.

620 53. Le SQ, Gascuel O. An improved general amino acid replacement matrix. Mol Biol
621 Evol. 2008;25(7):1307-20.

622 54. Zerbino DR, Achuthan P, Akanni W, Amode MR, Barrell D, Bhai J, et al. Ensembl
623 2018. Nucleic Acids Res. 2018;46(D1):D754-d61.

624 55. Eddy SR. Accelerated Profile HMM Searches. PLoS Comput Biol.
625 2011;7(10):e1002195.

626 56. Stanke M, Keller O, Gunduz I, Hayes A, Waack S, Morgenstern B. AUGUSTUS: ab
627 initio prediction of alternative transcripts. Nucleic Acids Res. 2006;34(Web Server
628 issue):W435-9.

629 57. Katoh K, Standley DM. MAFFT Multiple Sequence Alignment Software Version 7:
630 Improvements in Performance and Usability. Mol Biol Evol. 2013;30(4):772-80.

631 58. Nguyen LT, Schmidt HA, von Haeseler A, Minh BQ. IQ-TREE: A Fast and Effective
632 Stochastic Algorithm for Estimating Maximum-Likelihood Phylogenies. Mol Biol Evol.
633 2015;32(1):268-74.

634 59. Kalyaanamoorthy S, Minh BQ, Wong TKF, von Haeseler A, Jermiin LS.
635 ModelFinder: fast model selection for accurate phylogenetic estimates. Nat Methods.
636 2017;14(6):587-+.

637 60. Yang Z. PAML 4: phylogenetic analysis by maximum likelihood. Mol Biol Evol.
638 2007;24(8):1586-91.

639 61. Okonechnikov K, Golosova O, Fursov M, team tU. Unipro UGENE: a unified
640 bioinformatics toolkit. Bioinformatics. 2012;28(8):1166-7.

641 62. Goddard TD, Huang CC, Meng EC, Pettersen EF, Couch GS, Morris JH, et al. UCSF
642 ChimeraX: Meeting modern challenges in visualization and analysis. Protein Sci.
643 2018;27(1):14-25.

644 63. Waterhouse A, Bertoni M, Bienert S, Studer G, Tauriello G, Gumienny R, et al.
645 SWISS-MODEL: homology modelling of protein structures and complexes. Nucleic Acids
646 Res. 2018;46(W1):W296-W303.

647 64. Jumper J, Evans R, Pritzel A, Green T, Figurnov M, Ronneberger O, et al. Highly
648 accurate protein structure prediction with AlphaFold. Nature. 2021;596(7873):583-9.

649 65. Spielman SJ, Wilke CO. Pyvolve: A Flexible Python Module for Simulating
650 Sequences along Phylogenies. PloS one. 2015;10(9):e0139047.

651 66. Jones DT, Taylor WR, Thornton JM. The rapid generation of mutation data matrices
652 from protein sequences. Comput Appl Biosci. 1992;8(3):275-82.

653 67. Yang Z. A space-time process model for the evolution of DNA sequences. Genetics.
654 1995;139(2):993-1005.

655 68. Soubrier J, Steel M, Lee MS, Der Sarkissian C, Guindon S, Ho SY, et al. The
656 influence of rate heterogeneity among sites on the time dependence of molecular rates. Mol
657 Biol Evol. 2012;29(11):3345-58.

658 69. Saitou N, Nei M. The neighbor-joining method: a new method for reconstructing
659 phylogenetic trees. Mol Biol Evol. 1987;4(4):406-25.

660 70. Henikoff S, Henikoff JG. Amino acid substitution matrices from protein blocks. Proc
661 Natl Acad Sci U S A. 1992;89(22):10915-9.
662